International Journal of Non-Linear Mechanics 127 (2020) 103593

Contents lists available at ScienceDirect

International Journal of Non-Linear Mechanics

journal homepage: www.elsevier.com/locate/nlm

Bifurcation of a finitely deformed functionally graded dielectric elastomeric tube

Weijian Zhou [a], Yingjie Chen [b], Yipin Su [b,c,1,*]

[a] Department of Architecture and Civil Engineering, City university of Hong Kong, Hong Kong
[b] Department of Engineering Mechanics, Zhejiang University, Hangzhou 310027, PR China
[c] School of Mathematics, Statistics and Applied Mathematics, NUI Galway, University Road, Galway, Ireland

ARTICLE INFO

Keywords:
Functionally graded dielectric tube
Linearized buckling
Surface impedance matrix method
Neo-Hookean material

ABSTRACT

Soft functionally graded materials have attracted intensive attention owing to their special material inhomogeneity and are realized as various applications. In this paper, we theoretically investigate the finite deformation and superimposed bifurcation behaviors of an incompressible functionally graded dielectric tube subject to a combination of axial stretch and radial voltage. The theoretical framework of nonlinear electroelasticity and the related linearized incremental version is employed. We assume that the modulus and permittivity of the elastomer vary linearly along the thickness of the tube. The surface impedance matrix method is adopted to obtain the bifurcation equation for buckling of the tube. We present numerical calculation for the ideal neo-Hookean dielectric elastomer to study the effects of the applied voltage, geometrical size and material grading parameters on the nonlinear response and the incremental buckling behavior of the tube. We validate our results through comparison with those of the elastic problem. The results can provide solid guidance for the design and realization of dielectric actuators.

1. Introduction

Soft robotic actuators present many advantages compared with their rigid counterparts, including good sensitivity, high toughness, wide biocompatibility and softness, etc. [1]. However, soft actuators are unable to apply highly localized point loads. Recently, the so-called 'hybrid robots' composed of rigid and flexible components are proposed to overcome this limitation [2]. This kind of robots can grasp, puncture and anchor into solid components such as controller, chip and battery, owing to their rigid ends. On the other hand, these actuators are also compliant and resilient due to the soft parts, thus can be integrated with flexible and highly extensible devices [2,3].

One possible strategy for designing 'hybrid actuators' is to use multilayers composed of rigid and soft elastomers [2]. However, the circumferential stresses of the layers are discontinuous at the interface. As a result, interfacial slide, exfoliation and crack formation can be induced during the deformation. To overcome this potential problem, *functionally graded flexible actuators* have been developed for soft robotic applications [3,4].

Dielectric elastomers (DEs), as one class of highly deformable smart materials, have attracted considerable attention from both scientific and industrial community [5–9], attributing to their rapid and large deformation in response to external electric stimuli, reversible response, light weight, low cost, high reliability, etc. Their applications include actuators, transducers, biomechanical devices, tunable metamaterials, micro-pumps, as well as soft robots, artificial muscles, sensitive skins, and so on [10–14].

The DEs can be fabricated by embedding fine electroactive particles into rubber-like matrix [15]. Another simple way to produce DEs is to attach flexible electrodes onto the surfaces of a soft plate, tube or spherical shell [16]. Subject to an electrical voltage, the Coulomb force will be generated between the two electrodes with opposite charges so as to cause reduction in thickness and expansion in area of the actuator. Reports show that the voltage-induced strains in DEs can be over 100% [17].

Traditionally, functionally graded materials (FGMs) can be manufactured through well-established industrial processes, such as Plasma Spraying, Self-propagating High-temperature Synthesis (SHS), Powder Metallurgy Technique and Centrifugal Casting Method, etc. [18]. These methods can be extended for fabrication of functionally graded dielectric elastomers (FGDEs). For example, spatial inhomogeneities in chemical or mechanical properties can be introduced to rubber-like materials from the non-uniform temperature [19], and inhomogeneous

* Corresponding author at: School of Mathematics, Statistics and Applied Mathematics, NUI Galway, University Road, Galway, Ireland.
E-mail address: su_yp@zju.edu.cn (Y. Su).

[1] Accountable for all aspects of the work in ensuring that questions related to the accuracy or integrity of any part of the work are appropriately investigated and resolved.

https://doi.org/10.1016/j.ijnonlinmec.2020.103593
Received 30 April 2020; Received in revised form 21 August 2020; Accepted 22 August 2020
Available online 28 August 2020
0020-7462/

dielectric property can be realized by unevenly embedding electroactive particles into the FGM polymeric matrix through the multimaterial 3D printing technique [20].

Instabilities may occur in DEs when the applied voltage reaches a critical value, including electric breakdown, electromechanical instability (or pull-in instability) and bifurcation. Traditionally, the instabilities have been viewed as a main factor that causes the failure of the structure thus should be avoided in engineering. However, approaches have been proposed recently to design high-performance devices by utilizing instabilities of DE structures. For example, Wu et al. [13] utilized the instability-induced large deformation in DE phononic rod system to suddenly and widely tune the band gaps. Chen et al. [21] designed a periodic DE laminate with tunable band gaps utilizing the snap-through instability of the elastomer. Pang et al. [22] recently developed strategies to utilize buckling phenomenon in DEs for the electro-mechanically controlled 3D assembly.

The research of the large deformation in DEs is very challenging, mainly due to the multi-physical couplings and the strong nonlinearity. The theoretical framework of the nonlinear electroelasticity was first proposed in 1950s by Toupin [23]. Then, the theory was extended to include the thermal and magnetic coupling effects by Landau and Lifshitz [24], Tiersten [25], and Maugin [26], etc. Later, the linearized incremental theory is developed [27,28] for dealing with the small-on-large problems, e.g. the infinitesimal waves [29,30], vibration [31] and linearized buckling [32,33] in finitely deformed DE structures.

In the middle 1980s, a Japanese research group first proposed the concept of the FGMs, a new class of inhomogeneous materials with physical properties continuously varying along one or more directions [34]. Compared with layered structures [35], the continuous variation of the material properties enables the FGMs to eliminate the sharp stress discontinuity, avoid the high stress concentration, reduce the residual stress, increase the bonding strength, and at the same time remain the natural properties of each material constituent in them. The FGMs have been a hot research topic for decades, and a massive of works have been reported [36–39]. However, most of the existing researches on FGMs only deal with their linear mechanical responses or weak geometrical nonlinearity, but few of them [40,41] concern soft FGM structures with strong geometrical and material nonlinearity. In the present paper, we will concentrate on the analysis of nonlinear response and linearized buckling in FGDEs. Our purpose is to use the material gradient to optimize the nonlinear response and instability behavior of FGDE tubes.

We first derive the governing equations of large deformation in an FGDE tube subject to a radial voltage and an axial strain in Section 2. The shear modulus and permittivity of the elastomer are assumed to be graded along the thickness according to linear laws. Then in Section 3, we employ Dorfman and Ogden's incremental theory [28] to establish the bifurcation equations to predict and simulate the linearized buckling of the tube. The surface impedance matrix method is employed to obtain and solve the bifurcation equation. We present numerical results in Section 4 for ideal neo-Hookean DE material to discuss the influences of applied voltage, structural geometry and material gradient parameters on the finite response and incremental buckling behavior of the FGDE tube. We find that the application of voltage can help stabilize the FGDE tube, and the stabilization can be further enhanced by increasing the grading degree of permittivity and/or decreasing the grading degree of shear modulus. In addition, it can be seen that the influence of the permittivity gradient parameter on the buckling behavior of the tube is more notable than that of the modulus gradient parameter.

2. Finite deformation of an FGDE tube

2.1. Static motion

In this paper, we consider isotropic incompressible dielectric elastomers. Using the referential cylindrical system (R,Θ,Z), the FGDE tube originally occupies the region

$$R_i \le R \le R_o, \quad 0 \le \Theta \le 2\pi, \quad 0 \le Z \le L, \tag{2.1}$$

as illustrated in Fig. 1(a), where R_i and R_o are the inner and outer radii of the tube, respectively, L is the initial length. $\overline{R}_o = R_o/R_i$ is the dimensionless initial radius ratio and $H = R_o - R_i$ is the undeformed thickness of the tube. Throughout the paper, the physical parameters at the inner and outer faces of the tube are indicated with the subscripts 'i' and 'o', respectively.

Consider an FGDE tube with lateral ends attached with two paralleled rigid glossy plates. Subject to a voltage V across the thickness and a mechanical load along the length, the tube deforms finitely into the current region

$$r_i \le r \le r_o, \quad 0 \le \theta \le 2\pi, \quad 0 \le z \le l, \tag{2.2}$$

as illustrated in Fig. 1(b), through the following deformation [42,43]

$$R^2 - R_i^2 = \lambda_z(r^2 - r_i^2), \qquad \theta = \Theta, \qquad z = \lambda_z Z, \tag{2.3}$$

where λ_z is the uniform axial stretch of the tube. We adopt the notation $\bar{r}_o = r_o/r_i$ to denote the deformed radius ratio of the tube, with r_i and r_o being the inner and outer radii of the deformed tube, respectively. $l = \lambda_z L$ and $h = r_o - r_i$ are the length and thickness of the deformed tube, respectively. Here we focus on an incompressible FGDE tube maintaining its tubular shape when undergoing a combination of inflation and extension.

Then the deformation gradient $\boldsymbol{F}$ can be obtained from Eq. (2.3) as

$$\boldsymbol{F} = \frac{\partial \boldsymbol{x}}{\partial \boldsymbol{X}} = \begin{bmatrix} \lambda^{-1}\lambda_z^{-1} & 0 & 0 \\ 0 & \lambda & 0 \\ 0 & 0 & \lambda_z \end{bmatrix}, \tag{2.4}$$

where $\boldsymbol{x}$ and $\boldsymbol{X}$ are the position vectors of the material in the reference and deformed configurations, respectively, and $\lambda = r/R$ is the *circumferential stretch*, which from Eq. (2.3) reads

$$\lambda = \frac{1}{R}\sqrt{\frac{R^2 - R_i^2}{\lambda_z} + r_i^2}. \tag{2.5}$$

From Eqs. (2.3) and (2.5), we can obtain the relationship between the circumferential stretches at the inner and outer surfaces $\lambda_i = r_i/R_i$ and $\lambda_o = r_o/R_o$ and the axial stretch λ_z of the deformed tube as

$$\lambda_o = \frac{1}{\overline{R}_o}\sqrt{\frac{1}{\lambda_z}\left(\overline{R}_o^2 + \lambda_z\lambda_i^2 - 1\right)}, \tag{2.6}$$

and establish the following connections

$$\frac{\mathrm{d}r}{\mathrm{d}\lambda} = \frac{r}{\lambda\left(1 - \lambda_z\lambda^2\right)}, \quad R\mathrm{d}R = \lambda_z r\mathrm{d}r. \tag{2.7}$$

2.2. Electric and stress fields

The electric field in the solid is generated by applying a voltage through the flexible electrodes coated on the inner and outer faces of the dielectric tube. According to the Gauss's theorem, there is no exterior electric field and thus no Maxwell stress outside the tube [44].

On the basis of the nonlinear electroelasticity [32,45], the total Cauchy stress $\boldsymbol{\tau}$ and true electric field $\boldsymbol{E}$ in a deformed incompressible dielectric elastomer can be obtained as

$$\begin{aligned}\boldsymbol{\tau} = {} & 2\Omega_1\boldsymbol{b} + 2\Omega_2\left(I_1\boldsymbol{b} - \boldsymbol{b}^2\right) - p\boldsymbol{I} + 2\Omega_5\boldsymbol{D}\otimes\boldsymbol{D} \\ & + 2\Omega_6\left(\boldsymbol{D}\otimes\boldsymbol{b}\boldsymbol{D} + \boldsymbol{b}\boldsymbol{D}\otimes\boldsymbol{D}\right),\end{aligned} \tag{2.8}$$

$$\boldsymbol{E} = 2\left(\Omega_4\boldsymbol{b}^{-1}\boldsymbol{D} + \Omega_5\boldsymbol{D} + \Omega_6\boldsymbol{b}\boldsymbol{D}\right), \tag{2.9}$$

where $\boldsymbol{D}$ is the true electric displacement, $\boldsymbol{I}$ is identity tensor, $\boldsymbol{b} = \boldsymbol{F}\boldsymbol{F}^{\mathrm{T}}$ is the left Cauchy–Green deformation tensor, and p is a Lagrange multiplier associated with the incompressibility constraint of the solid, which can be determined from the boundary conditions. Here the

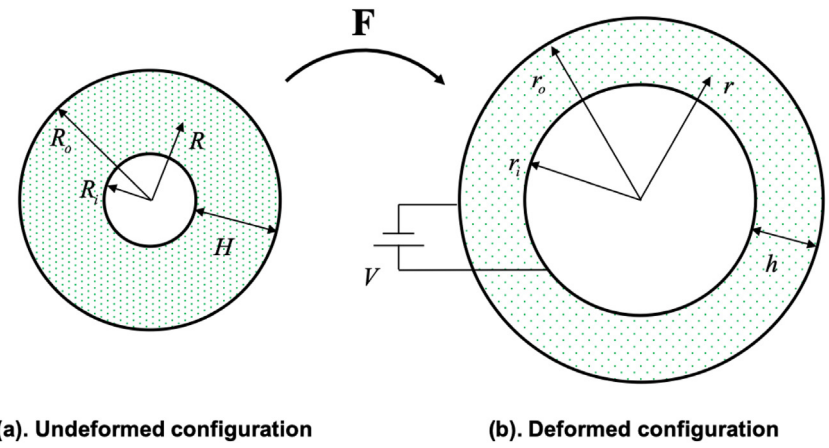

Fig. 1. Sketch of the in-plane cross section of an FGDE tube in the (a) undeformed and (b) deformed configurations.

shorthand notation $\Omega_m = \partial\Omega/\partial I_m$ $(m = 1,2,4,5,6)$ is adopted, with $\Omega(I_1, I_2, I_4, I_5, I_6)$ being the augmented free energy function of the elastomer, which can be expressed in terms of the following five invariants

$$I_1 = \mathrm{tr}\boldsymbol{c}, \quad I_2 = \mathrm{tr}\left(\boldsymbol{c}^{-1}\right), \quad I_4 = \boldsymbol{D}_l \cdot \boldsymbol{D}_l,$$
$$I_5 = \boldsymbol{D}_l \cdot \boldsymbol{c}\boldsymbol{D}_l, \quad I_6 = \boldsymbol{D}_l \cdot \boldsymbol{c}^2\boldsymbol{D}_l, \tag{2.10}$$

where $\boldsymbol{c} = \boldsymbol{F}^{\mathrm{T}}\boldsymbol{F}$ is the right Cauchy–Green deformation tensor and $\boldsymbol{D}_l = \boldsymbol{F}^{-1}\boldsymbol{D}$ is the nominal electric displacement.

For the considered problem, the nominal electric field and electric displacement have the forms

$$\boldsymbol{E}_l = \begin{bmatrix} E_R & 0 & 0 \end{bmatrix}^{\mathrm{T}}, \quad \boldsymbol{D}_l = \begin{bmatrix} D_R & 0 & 0 \end{bmatrix}^{\mathrm{T}}, \tag{2.11}$$

where E_R and D_R are the only non-zero components of the nominal electric field and electric displacement along the radial direction, respectively.

Then the true electric field and electric displacement can be obtained as

$$\boldsymbol{E} = \boldsymbol{F}^{-T}\boldsymbol{E}_l = \begin{bmatrix} E_r & 0 & 0 \end{bmatrix}^{\mathrm{T}}, \quad \boldsymbol{D} = \boldsymbol{F}\boldsymbol{D}_l = \begin{bmatrix} D_r & 0 & 0 \end{bmatrix}^{\mathrm{T}}, \tag{2.12}$$

where $E_r = \lambda\lambda_z E_R$ and $D_r = \lambda^{-1}\lambda_z^{-1} D_R$ are the only non-zero components of the true electric field and electric displacement along the radial direction, respectively.

The non-zero components of the total Cauchy stress $\boldsymbol{\tau}$ and of the electric field $\boldsymbol{E}$ can be derived from Eqs. (2.4) and (2.8)–(2.12) as

$$\tau_{rr} = 2\lambda^{-2}\lambda_z^{-2}\Omega_1 + 2\left(\lambda^{-2} + \lambda_z^{-2}\right)\Omega_2 + 2\lambda^{-2}\lambda_z^{-2}D_R^2\Omega_5 + 4\lambda^{-4}\lambda_z^{-4}D_R^2\Omega_6 - p,$$
$$\tau_{\theta\theta} = 2\lambda^2\Omega_1 + 2\left(\lambda_z^{-2} + \lambda^2\lambda_z^2\right)\Omega_2 - p,$$
$$\tau_{zz} = 2\lambda_z^2\Omega_1 + 2\left(\lambda^{-2} + \lambda^2\lambda_z^2\right)\Omega_2 - p, \tag{2.13}$$
$$E_r = 2\left(\lambda\lambda_z\Omega_4 + \lambda^{-1}\lambda_z^{-1}\Omega_5 + \lambda^{-3}\lambda_z^{-3}\Omega_6\right)D_R. \tag{2.14}$$

Introducing a reduced energy function W defined by

$$W\left(\lambda, \lambda_z, D_R\right) = \Omega\left(I_1, I_2, I_4, I_5, I_6\right), \tag{2.15}$$

Eqs. (2.13) and (2.14) yield the following relationships:

$$\tau_{rr} - \tau_{\theta\theta} = -\lambda\frac{\partial W}{\partial\lambda}, \qquad \tau_{rr} - \tau_{zz} = -\lambda_z\frac{\partial W}{\partial\lambda_z}, \tag{2.16}$$

$$E_R = \lambda^{-1}\lambda_z^{-1}E_r = \frac{\partial W}{\partial D_R}. \tag{2.17}$$

Specifically, we consider *ideal dielectric elastomers* with the energy function [46,47]

$$W(\lambda, \lambda_z, D_R) = W^E(\lambda, \lambda_z) + \frac{D_R^2}{2\varepsilon\lambda^2\lambda_z^2}. \tag{2.18}$$

Here the first term W^E on the righthand is the elastic energy of the elastomer which generally contains the shear modulus μ, and the second term containing the permittivity ε accounts for the interaction between the finite deformation and the electric displacement field. The shear modulus μ and the permittivity ε of the elastomer are taken to be graded in the thickness direction according to the following linear laws [40,41]

$$\mu(R) = \mu^0\left(1 + \beta^\mu\overline{R}\right), \quad \varepsilon(R) = \varepsilon^0\left(1 - \beta^\varepsilon\overline{R}\right), \tag{2.19}$$

where

$$\overline{R}(\lambda) = R/R_i = \sqrt{\frac{1 - \lambda_z\lambda_i^2}{1 - \lambda_z\lambda^2}}, \tag{2.20}$$

μ^0 and ε^0 are material constants, β^μ and β^ε are two dimensionless parameters characterizing the functionally graded properties of the elastomer, respectively.

For ideal dielectric elastomers, from Eqs. (2.17) and (2.18) and the relationship $E_r = \lambda\lambda_z E_R$ we have [32,48]

$$D_r = \varepsilon E_r. \tag{2.21}$$

Note that the true electric displacement component D_r satisfies the relationship [32]

$$rD_r \equiv \text{constant}, \tag{2.22}$$

which follows from the Maxwell equation

$$\mathrm{div}\boldsymbol{D} = \frac{1}{r}\frac{\partial(rD_r)}{\partial r} = 0. \tag{2.23}$$

The electric potential difference between the inner and outer surfaces of the tube is

$$V = \int_{r_i}^{r_o} E_r\,\mathrm{d}r. \tag{2.24}$$

From Eqs. (2.19)–(2.24), we can express the electric displacement as

$$\overline{D}_R = \frac{\overline{V}\lambda_z\left(\overline{R}_o - 1\right)}{f(\lambda_o)}\sqrt{\frac{1 - \lambda_z\lambda^2}{1 - \lambda_z\lambda_i^2}}, \tag{2.25}$$

where

$$f(\lambda) = \int_{\lambda_i}^{\lambda}\frac{1}{1 - \beta^\varepsilon\overline{R}}\frac{\mathrm{d}\lambda}{\lambda\left(1 - \lambda_z\lambda^2\right)}, \tag{2.26}$$

and

$$\overline{D}_R = \frac{D_R}{\sqrt{\varepsilon^0\mu^0}}, \quad \overline{V} = \frac{V}{R_o - R_i}\sqrt{\frac{\mu^0}{\varepsilon^0}} \tag{2.27}$$

are non-dimensional measurements of D_R and V, respectively.

According to the nonlinear electroelasticity, the equilibrium equations of the tube reduce to [32,45]

$$\frac{\partial \tau_{rr}}{\partial r}+\frac{1}{r}\left(\tau_{rr}-\tau_{\theta\theta}\right)=0, \tag{2.28}$$

where τ_{ii} $(i=r,\theta,z)$ are the non-zero components of the total Cauchy stress.

The radial stress τ_{rr} can be obtained from Eqs. (2.7), $(2.16)_1$ and (2.28) as

$$\tau_{rr}=\int_{\lambda_i}^{\lambda}\frac{\partial W}{\partial \lambda}\frac{1}{1-\lambda_z\lambda^2}\,\mathrm{d}\lambda+\tau_{rr}(r_i). \tag{2.29}$$

For the considered problem, the inner and outer faces of the tube are taken to be traction-free, i.e.

$$\tau_{rr}(r_i)=\tau_{rr}(r_o)=0. \tag{2.30}$$

Combining Eqs. (2.18), (2.25), (2.29) and the boundary condition (2.30), the voltage $\overline{V}$ can be expressed as

$$\overline{V}=\frac{|f(\lambda_o)|}{\lambda_z\left(\overline{R}_o-1\right)}\sqrt{\frac{\left(\lambda_z\lambda_i^2-1\right)h(\lambda_o)}{g(\lambda_o)}} \tag{2.31}$$

where

$$g(\lambda)=\left[2\overline{\varepsilon}(\lambda)\lambda^2\lambda_z^2\right]^{-1}-\left[2\overline{\varepsilon}(\lambda_i)\lambda_i^2\lambda_z^2\right]^{-1},$$
$$h(\lambda)=\int_{\lambda_i}^{\lambda}\frac{\partial \overline{W}^{E}(\lambda,\lambda_z)}{\partial\lambda}\frac{\mathrm{d}\lambda}{1-\lambda_z\lambda^2}. \tag{2.32}$$

with

$$\overline{\varepsilon}=\frac{\varepsilon}{\varepsilon^0},\qquad \overline{W}^{E}=\frac{W^E}{\mu^0} \tag{2.33}$$

being the non-dimensional measurements of ε and W^E, respectively.

Finally, the inner and outer circumferential stretches λ_i and λ_o of the FGDE tube can be determined by solving Eqs. (2.6) and (2.31), once the axial stretch λ_z and applied voltage $\overline{V}$ are given.

From Eqs. (2.29) and (2.31), the dimensionless radial stress is

$$\overline{\tau}_{rr}(\lambda)=\frac{\tau_{rr}}{\mu^0}=h(\lambda)+\frac{1}{1-\lambda_z\lambda_i^2}\left[\frac{\overline{V}\lambda_z\left(\overline{R}_o-1\right)}{f(\lambda_o)}\right]^2 g(\lambda). \tag{2.34}$$

Then the full stress distribution in the deformed tube can be determined from Eqs. (2.16) and (2.34).

The axial mechanical load applied at the end of the tube is [43,49]

$$F=2\pi\int_{r_i}^{r_o}\tau_{zz}r\,\mathrm{d}r=\pi\int_{r_i}^{r_o}\left(2\lambda_z\frac{\partial W}{\partial\lambda_z}-\lambda\frac{\partial W}{\partial\lambda}\right)r\,\mathrm{d}r. \tag{2.35}$$

3. Bifurcation analysis

Upon the finitely deformed configuration, we superimpose a small 3D harmonic inhomogeneous incremental deformation $\boldsymbol{u}=\boldsymbol{u}(\boldsymbol{x})$ along with an incremental electric displacement $\dot{\boldsymbol{D}}$, with components in the form [32,50]

$$\begin{aligned}
u_r&=U_r(r)\cos(n\theta)\cos(kz), & u_\theta&=U_\theta(r)\sin(n\theta)\cos(kz),\\
u_z&=U_z(r)\cos(n\theta)\sin(kz), & \dot{\phi}&=\Phi(r)\cos(n\theta)\cos(kz),\\
\dot{T}_{rr}&=\Sigma_{rr}(r)\cos(n\theta)\cos(kz), & \dot{T}_{r\theta}&=\Sigma_{r\theta}(r)\sin(n\theta)\cos(kz),\\
\dot{T}_{rz}&=\Sigma_{rz}(r)\cos(n\theta)\sin(kz), & \dot{D}_r&=\Delta_r(r)\cos(n\theta)\cos(kz),
\end{aligned} \tag{3.1}$$

where u_r,u_θ,u_z and $\dot{T}_{rr},\dot{T}_{r\theta},\dot{T}_{zz}$ are components of $\boldsymbol{u}$ and the push-forward form of incremental nominal stress $\dot{\boldsymbol{T}}$, respectively, and $\dot{D}_r$ is component of the push-forward form of incremental electric displacement in the r-direction. The incremental electric potential $\dot{\phi}$ is introduced such that the incremental electric field can be expressed as $\dot{\boldsymbol{E}}=-\mathrm{grad}\dot{\phi}$. $U_r,U_\theta,U_z,\Phi,\Sigma_{rr},\Sigma_{r\theta},\Sigma_{rz}$ and Δ_r are scalar functions of r only, n is the *circumferential wavenumber*, and k is the *axial wavenumber*.

Hereinafter, incremental quantities are identified by a superimposed dot.

We assume that the tube is subject to an end thrust at the faces $z=0,l$, while the two surfaces $r=r_i,r_o$ remain traction-free and the applied voltage is taken to be a constant. Then the incremental boundary conditions for the incremental fields are

$$\begin{aligned}
&u_z=\dot{T}_{0zr}=\dot{T}_{0z\theta}=0 && \text{at}\quad z=0,\lambda_z L,\\
&\dot{T}_{0rr}=\dot{T}_{0r\theta}=\dot{T}_{0rz}=\dot{\phi}=0 && \text{at}\quad r=r_i,r_o.
\end{aligned} \tag{3.2}$$

Combining Eqs. (3.1) and $(3.2)_1$ yields the relationship between the wavenumber k and the length of the tube L as

$$k=\frac{m\pi}{\lambda_z L}\quad (m=0,1,2,\ldots). \tag{3.3}$$

The governing equations of the incremental motion can be recast in the form of the following first-order differential system [32]

$$\frac{\mathrm{d}}{\mathrm{d}r}\boldsymbol{\eta}(r)=\frac{1}{r}\boldsymbol{G}\boldsymbol{\eta}(r), \tag{3.4}$$

where $\boldsymbol{\eta}(r)=\left[U_r\quad U_\theta\quad U_z\quad r\Delta_r\quad r\Sigma_{rr}\quad r\Sigma_{r\theta}\quad r\Sigma_{rz}\quad \Phi\right]^{\mathrm{T}}=\left[\boldsymbol{U}\quad \boldsymbol{S}\right]^{\mathrm{T}}$ is the Stroh vector (with $\boldsymbol{U}=\left[U_r\quad U_\theta\quad U_z\quad r\Delta_r\right]^{\mathrm{T}}$ and $\boldsymbol{S}=\left[r\Sigma_{rr}\quad r\Sigma_{r\theta}\quad r\Sigma_{rz}\quad \Phi\right]^{\mathrm{T}}$), and $\boldsymbol{G}$ is the so-called Stroh matrix, with its components given in Appendix A.

According to the standard *surface impedance matrix method* [32,51], the bifurcation relation of the buckled tube can be obtained by solving the so-called Riccati differential equation

$$\frac{\mathrm{d}\boldsymbol{z}^i}{\mathrm{d}r}=\frac{1}{r}\left(-\boldsymbol{z}^i\boldsymbol{G}_1-\boldsymbol{z}^i\boldsymbol{G}_2\boldsymbol{z}^i+\boldsymbol{G}_3+\boldsymbol{G}_4\boldsymbol{z}^i\right), \tag{3.5}$$

with the initial and stop conditions

$$\boldsymbol{z}^i(r_i,r_i)=\boldsymbol{0},\qquad \det\boldsymbol{z}^i(r_o,r_i)=0, \tag{3.6}$$

which can be derived from the incremental boundary conditions (3.2). Here the components of the matrices $\boldsymbol{G}_1\sim\boldsymbol{G}_4$ are given in Appendix A, and $\boldsymbol{z}^i(r,r_i)$ is the so-called conditional impedance matrix, linking the traction and the displacement vectors as

$$\boldsymbol{S}(r)=\boldsymbol{z}^i(r,r_i)\boldsymbol{U}(r). \tag{3.7}$$

4. Numerical results

4.1. Material model

The particular form of energy function we consider here is the neo-Hookean dielectric model given by [47,52]

$$W(\lambda,\lambda_z,D_R)=W^E(\lambda,\lambda_z)+\frac{D_R^2}{2\lambda^2\lambda_z^2\varepsilon}=\frac{\mu}{2}(\lambda^2+\lambda^{-2}\lambda_z^{-2}+\lambda_z^2-3)+\frac{D_R^2}{2\lambda^2\lambda_z^2\varepsilon} \tag{4.1}$$

where $\mu(\lambda)$ and $\varepsilon(\lambda)$ are the shear modulus and the permittivity of the elastomer, respectively, given by Eq. (2.19).

Then the functions $f(\lambda)$, $g(\lambda)$ and $h(\lambda)$ can be calculated as [41]

$$\begin{aligned}
f(\lambda)&=a\ln\frac{x+\overline{R}}{x+1}+b\left(\tan^{-1}\frac{\overline{R}}{\sqrt{y}}-\tan^{-1}\frac{1}{\sqrt{y}}\right)-a\ln\left(\frac{\lambda}{\lambda_i}\sqrt{\frac{1-\lambda_z\lambda_i^2}{1-\lambda_z\lambda^2}}\right),\\
g(\lambda)&=\frac{1}{2\lambda_z^2\lambda_i^2\left(\beta^{\varepsilon}-1\right)}+\frac{1}{2\lambda_z^2\lambda^2\left(1-\beta^{\varepsilon}\sqrt{\frac{\lambda_i^2\lambda_z^2-1}{\lambda^2\lambda_z^2-1}}\right)},\\
h(\lambda)&=-\frac{1}{\lambda_z}\left[\ln\lambda+\frac{G(1+\beta^{\mu})}{2\overline{r}^2}-\frac{3\beta^{\mu}\sqrt{\lambda_z G}}{2}\tan^{-1}\frac{\overline{R}}{\sqrt{\lambda_z G}}\right]\\
&\quad+\frac{1}{\lambda_z}\left[\ln\lambda_i+\frac{G(1+\beta^{\mu})}{2\lambda_i^2}-\frac{3\beta^{\mu}\sqrt{\lambda_z G}}{2}\tan^{-1}\frac{\overline{R}}{\sqrt{\lambda_z G}}\right],
\end{aligned} \tag{4.2}$$

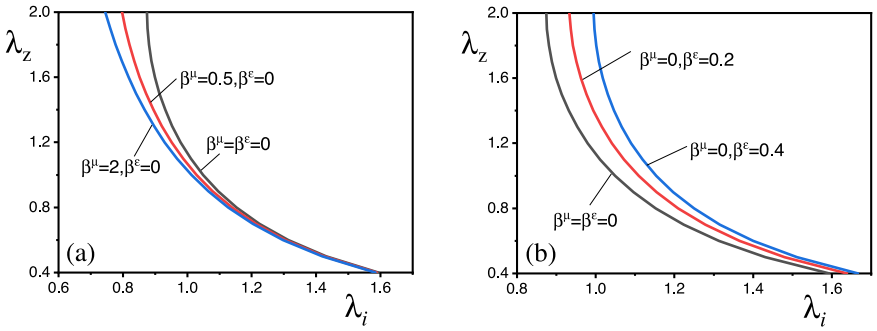

Fig. 2. Effects of (a) modulus gradient parameter β^{μ} and (b) permittivity gradient parameter β^{ε} on the nonlinear response of an FGDE tube with $\overline{R}_o = 2$ subject to a voltage $\overline{V} = 0.3$.

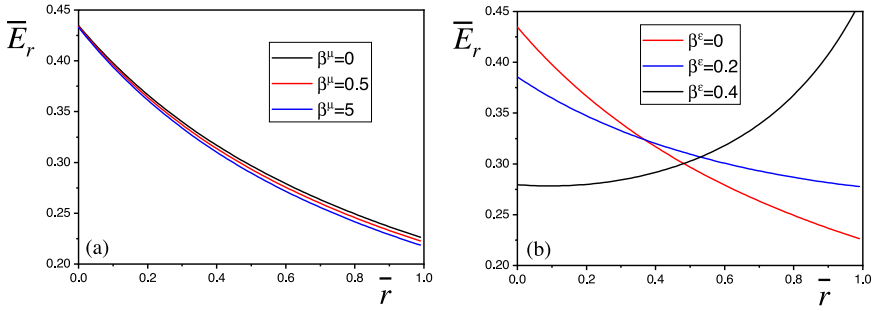

Fig. 3. Plots of $\overline{E}_r$ versus $\bar{r}$ of an FGDE tube with $\overline{R}_o = 2$ and varying (a) modulus gradient parameter β^{μ} and (b) permittivity gradient parameter β^{ε} subject to a voltage $\overline{V} = 0.3$ and an axial stretch $\lambda_z = 1$.

where

$$x = -\frac{1}{\beta^{\varepsilon}} \qquad y = \lambda_z \lambda_i^2 - 1,$$

$$a = \frac{1}{(\beta^{\varepsilon})^2\left(1-\lambda_i^2\lambda_z\right)-1}, \qquad b = \frac{\beta^{\varepsilon}\left(1-\lambda_i^2\lambda_z\right)}{\sqrt{\lambda_i^2\lambda_z - 1}\left[(\beta^{\varepsilon})^2\left(1-\lambda_i^2\lambda_z\right)-1\right]},$$

$$G = \lambda_i^2 - \lambda_z^{-1}, \qquad \bar{r} = \frac{r}{R_i} = \lambda\sqrt{\frac{1-\lambda_z\lambda_i^2}{1-\lambda_z\lambda^2}}. \tag{4.3}$$

The components of the electroelastic moduli tensors for the ideal neo-Hookean dielectrics can be obtained by substituting Eq. (4.1) into Appendix B as

$$\mathcal{A}_{1111} = \mathcal{A}_{1212} = \frac{D_r^2}{\varepsilon} + \frac{\mu}{\lambda^2\lambda_z^2}, \qquad \mathcal{A}_{1122} = \mathcal{A}_{1221} = 0,$$

$$\mathcal{A}_{2222} = \mathcal{A}_{2121} = \mu\lambda^2,$$

$$\Gamma_{122} = \frac{D_r}{\varepsilon}, \qquad K_{22} = \frac{1}{\varepsilon}. \tag{4.4}$$

Note that the material parameters μ and ϵ in Eq. (4.4) are functions of the stretch λ.

4.2. Nonlinear response

Fig. 2 presents the nonlinear response of an FGDE tube with the radius ratio $\overline{R}_o = 2$ for different material gradient parameters β^{μ} and β^{ε}, subject to a fixed electric voltage $\overline{V} = 0.3$. The inner circumferential stretch λ_i decreases as the axial stretch λ_z increases, which is independent of β^{μ} and β^{ε}. Particularly, for tubes with a larger value of β^{μ} or a smaller value of β^{ε}, an identical axial stretch λ_z will result in a smaller circumferential stretch λ_i. It can be seen that the effects of β^{μ} and β^{ε} on the finite deformation of the tube can be ignored for large value of λ_i.

Fig. 3 displays the effects of the material gradient parameters β^{μ} and β^{ε} on the distribution of the dimensionless true electric field $\overline{E}_r = E_r\sqrt{\varepsilon^0/\mu^0}$ through the thickness $\bar{r} = (r - r_i)/(r_o - r_i)$ of an FGDE tube with $\overline{R}_o = 2$ subject to a radial voltage $\overline{V} = 0.3$ and an axial stretch $\lambda_z = 1$. It can be seen that for a homogeneous tube with $\beta^{\mu} = \beta^{\varepsilon} = 0$, the true electric field $\overline{E}_{ri}$ at the face r_i is always higher than the true electric field $\overline{E}_{ro}$ at the face r_o, which, in fact, can be obtained from Eqs. (2.21) and (2.22). It means that electric breakdown [53,54] may occur first at the inner face of the tube once $\overline{E}_{ri}$ reaches the dielectric strength of the elastomer. Fig. 3*a* shows that increasing β^{μ} can slightly decrease the true electric field in the tube, but the maximum electric field still occur at the inner face of the tube. Particularly, the increase of β^{ε} can decrease the electric field at the inner face and increase that at the outer face of the tube (Fig. 3*b*). Keeping increasing β^{ε} will finally make the electric field at the outer face of the tube higher than that at the inner face. This provides guidance for the design of DE actuators where the active devices are placed on the inner part.

4.3. Bifurcation instability

We first validate our calculation by recovering the purely elastic problem which has been previously investigated [55]. Fig. 4 presents the bifurcation curves of an elastic tube ($\overline{V} = 0$) with $\overline{R}_o = 2$ for different circumferential mode numbers $n = 0{-}3$. A series of bifurcation branches can be solved from the bifurcation equation (3.5) by taking $n = 0, 1, 2, 3$. Multiple instability modes occur for a given wavenumber $\overline{k} = k(R_o - R_i)$, when the axial stretch λ_z reaches different critical values. However only the largest value corresponding to the onset of the instability is meaningful, as highlighted by the thicker stroke. It can be seen that the Euler buckling mode $n = 1$ occurs first for a slender tube with small $\overline{k}$ while the first barreling mode $n = 0$ becomes the dominant buckling mode for a short tube with large $\overline{k}$. The critical axial stretch approaches to the asymptotic value $\lambda_c = 0.444$ as the $\overline{k}$ increases, corresponding to the surface instability of a compressed elastic slab [56].

Fig. 5 reports the critical stretch λ_z^c as a function of the wavenumber $\overline{k}$ for FGDE tubes with $\beta^{\mu} = 1$, $\beta^{\varepsilon} = 0.2$, and different radius ratios (a) $\overline{R}_o = 2$ and (b) $\overline{R}_o = 1.05$ subject to a voltage $\overline{V} = 0.5$. It can be seen that

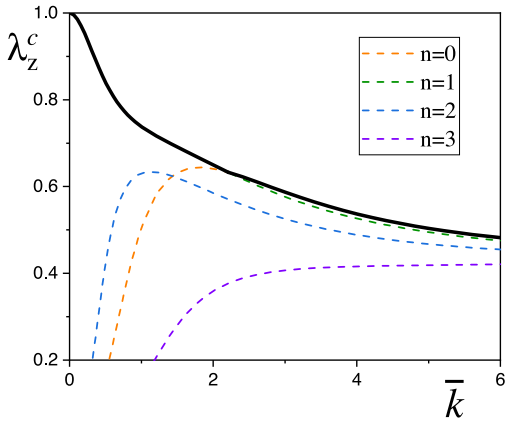

Fig. 4. Plots of the critical axial stretch λ_z^c versus dimensionless wavenumber $\bar{k}$ for a range of mode numbers $n = 0, 1, 2, 3$ for an elastic tube with $\bar{R}_o = 2$, $\beta^\mu = \beta^\varepsilon = 0$ and $\bar{V} = 0$. The instability of the tube will be triggered when the applied axial stretch λ_z reaches the highest value of the buckling branches, as highlighted by the black solid curve.

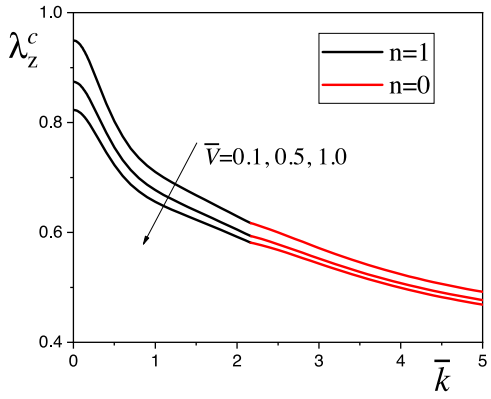

Fig. 6. Plots of λ_z^c versus $\bar{k}$ for an FGDE tube with $\bar{R}_o = 2$, $\beta^\mu = 1$, $\beta^\varepsilon = 0.2$ subject to voltages $\bar{V} = 0.1, 0.5, 1.0$.

a thin tube with small $\bar{R}_o$ is more susceptible to bifurcation instability. For thick tubes with relatively large $\bar{R}_o$, the dominant buckling mode switches from $n = 1$ to $n = 0$, and the onset value of axial stretch λ_z^c for instability decreases monotonously to the asymptotic value as the wavenumber $\bar{k}$ increases. While for thin tubes with small $\bar{R}_o$, the true buckling curve is non-monotonic. In this case, higher buckling modes ($n \geq 2$) can be induced, depending on the wavenumber $\bar{k}$ [55]. In Fig. 5*b*, as the wavenumber $\bar{k}$ increases, the dominant buckling mode of the tube switches from $n = 1$ to $n = 2$ to $n = 3$ and then back to $n = 2$ to $n = 1$ until to $n = 0$. It can be expected that for a thinner FGDE tube ($\bar{R}_o < 1.05$), the dominant buckling mode will vary according to the rule $n = 1 \to 2 \to 3 \to \ldots \to N \to \ldots \to 3 \to 2 \to 1 \to 0$, where N is the highest buckling mode of the tube, as the wavenumber $\bar{k}$ increases. That is, a slender tube always buckles in the mode $n = 1$ and a short and thick tube always buckles in the mode $n = 0$.

In Fig. 6 we examine the effect of the applied voltage $\bar{V}$ on the bifurcation behavior of a tube with $\bar{R}_o = 2$, $\beta^\mu = 1$, $\beta^\varepsilon = 0.2$. Here only the meaningful true critical axial stretch for bifurcation is presented. It can be seen that the critical axial stretch λ_z^c decreases as the applied voltage $\bar{V}$ increases. That is, the application of an electric voltage stabilizes the FGDE tube.

Fig. 7 presents the effect of the gradient parameters β^μ and β^ε on the $\lambda_z^c - \bar{k}$ plots. Results show that the stability of the tube can be enhanced by increasing β^ε and/or decreasing β^μ. Moreover, the influence of the permittivity gradient parameter β^ε on the buckling behavior of the tube is more notable than that of the modulus gradient parameter β^μ. Thus tuning the permittivity gradient parameter β^ε is a proper approach to enhance the stability of the elastomer.

5. Conclusion

In conclusion, we presented a theoretical analysis of the finite deformation and the associated bifurcation behavior of an FGDE tube subject to a radial voltage and an axial stretch. We derived explicit expressions of the biasing electric and mechanical fields in the finitely deformed ideal neo-Hookean FGDE tube. The modulus and permittivity of the elastomer are taken to vary linearly in the direction of the thickness. We used the linearized incremental theory to study the incremental motion superposed on the finitely deformed configuration and adopted the standard robust surface impedance matrix method to solve the resulting incremental boundary problem.

We studied the influences of the applied voltage, structural geometry and material gradient parameters on the nonlinear response and incremental buckling behavior of an FGDE tube. Results show that a long thick tube will buckle in the Euler buckling mode ($n = 1$) while a short thick tube will buckle in the barreling mode ($n = 0$). However, higher buckling modes ($n \geq 2$) can be induced for a thin tube, depending on the wavenumber. We found that the application of the voltage stabilizes the tube and this stabilization can be enhanced by increasing β^ε and/or decreasing β^μ.

Recent experimental observation [57] and finite element simulation [58] have been proposed to validate the theoretical prediction of linearized perturbation analysis of instability of finitely deformed soft elastic tubes. To the best knowledge of the authors, experimental or FEM study on the effects of the applied voltage and material gradient properties on instability of FGDE tubes is still lacking. The current

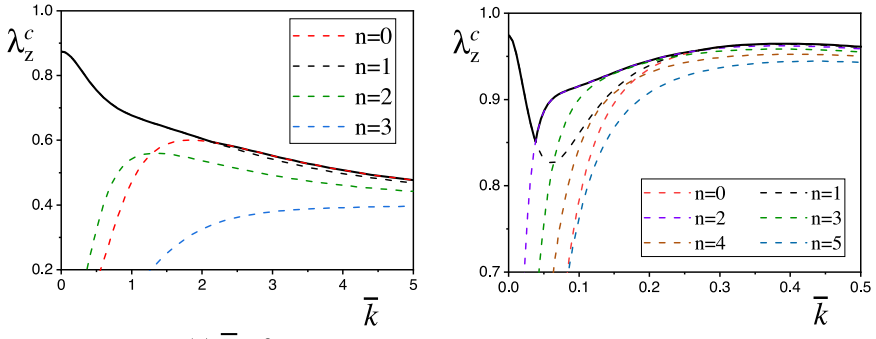

Fig. 5. Effect of the radius ratio $\bar{R}_o$ on the bifurcation behavior of an FGDE tube with $\beta^\mu = 1.0$ and $\beta^\varepsilon = 0.2$ subject to an electric voltage $\bar{V} = 0.5$. Higher buckling mode may occur in the tube with small $\bar{R}_o$.

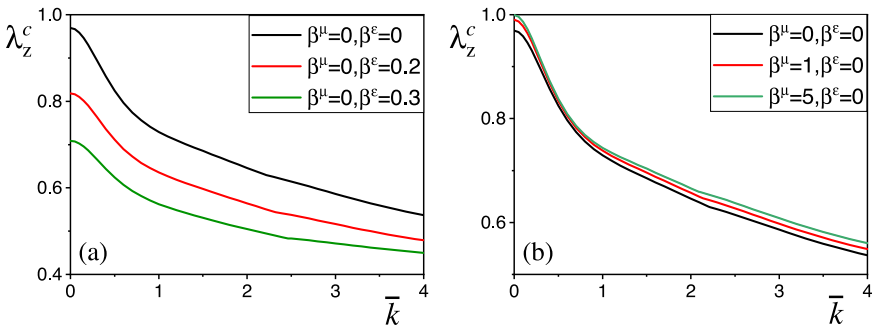

Fig. 7. Effects of (a) modulus gradient parameter β^μ and (b) permittivity gradient parameter β^ϵ on the bifurcation behavior of an FGDE tube with $\overline{R}_o = 2$ subject to a fixed voltage $\overline{V} = 0.3$.

work can be expanded in the future by comparing the theoretical, experimental and numerical results.

CRediT authorship contribution statement

Weijian Zhou: Developed mechanics modeling and analysis, Read and contributed to the manuscript. **Yingjie Chen:** Performed numerical calculations, Read and contributed to the manuscript. **Yipin Su:** Conceived and designed the work, Developed mechanics modeling and analysis, Read and contributed to the manuscript.

Declaration of competing interest

The authors declare that they have no known competing financial interests or personal relationships that could have appeared to influence the work reported in this paper.

Acknowledgments

This work was supported by the Government of Ireland Postdoctoral Fellowship from the Irish Research Council, Ireland (No. GOIPD/2017/1208), the China Scholarship Council and the Zhejiang Provincial Natural Science Foundation of China for Young Scholars (LQ20A020009). YPS acknowledges the support from the Shenzhen Scientific and Technological Fund for R&D, China (No. JCYJ20170816172316775).

Appendix A. Components of the Stroh matrix

The Stroh matrix $\boldsymbol{G}$ in Eq. (3.4) can be simplified as

$$\boldsymbol{G} = \begin{bmatrix} \boldsymbol{G}_1 & \boldsymbol{G}_2 \\ \boldsymbol{G}_3 & \boldsymbol{G}_4 \end{bmatrix}, \tag{A.1}$$

where the four 4×4 sub-blocks $\boldsymbol{G}_1, \boldsymbol{G}_2, \boldsymbol{G}_3$ and $\boldsymbol{G}_4$ have the following components [32]

$$\boldsymbol{G}_1 = \begin{bmatrix} -1 & -n & -kr & 0 \\ \frac{n(\gamma_{12}-\tau_{rr})}{\gamma_{12}} & \frac{\gamma_{12}-\tau_{rr}}{\gamma_{12}} & 0 & 0 \\ \frac{kr(\gamma_{13}-\tau_{rr})}{\gamma_{13}} & 0 & 0 & 0 \\ \xi_1 & -\frac{n\tau_{rr}}{\gamma_{12}}\frac{\Gamma_{122}}{K_{22}} & 0 & 0 \end{bmatrix},$$

$$\boldsymbol{G}_2 = \begin{bmatrix} 0 & 0 & 0 & 0 \\ 0 & \frac{1}{\gamma_{12}} & 0 & -\frac{n}{\gamma_{12}}\frac{\Gamma_{122}}{K_{22}} \\ 0 & 0 & \frac{1}{\gamma_{13}} & -\frac{kr}{\gamma_{13}}\frac{\Gamma_{133}}{K_{33}} \\ 0 & \frac{n}{\gamma_{12}}\frac{\Gamma_{122}}{K_{22}} & \frac{kr}{\gamma_{13}}\frac{\Gamma_{133}}{K_{33}} & \xi_2 \end{bmatrix},$$

$$\boldsymbol{G}_3 = \begin{bmatrix} \kappa_{11} & \kappa_{12} & \kappa_{13} & -\left(\Gamma_{111}-\Gamma_{221}\right) \\ \kappa_{12} & \kappa_{22} & \kappa_{23} & -n\left(\Gamma_{111}-\Gamma_{221}\right) \\ \kappa_{13} & \kappa_{23} & \kappa_{33} & -kr\left(\Gamma_{111}-\Gamma_{331}\right) \\ \Gamma_{111}-\Gamma_{221} & n\left(\Gamma_{111}-\Gamma_{221}\right) & kr\left(\Gamma_{111}-\Gamma_{331}\right) & -K_{11} \end{bmatrix},$$

$$\boldsymbol{G}_4 = \begin{bmatrix} 1 & -\frac{n(\gamma_{12}-\tau_{rr})}{\gamma_{12}} & -\frac{kr(\gamma_{13}-\tau_{rr})}{\gamma_{13}} & \xi_1 \\ n & -\frac{\gamma_{12}-\tau_{rr}}{\gamma_{12}} & 0 & -\frac{n\tau_{rr}}{\gamma_{12}}\frac{\Gamma_{122}}{K_{22}} \\ kr & 0 & 0 & 0 \\ 0 & 0 & 0 & 0 \end{bmatrix}, \tag{A.2}$$

where

$$\gamma_{12} = \mathcal{A}_{1212} - \frac{\Gamma_{122}^2}{K_{22}}, \quad \gamma_{21} = \mathcal{A}_{2121} - \frac{\Gamma_{122}^2}{K_{22}}, \quad \gamma_{23} = \mathcal{A}_{2323},$$

$$\gamma_{13} = \mathcal{A}_{1313} - \frac{\Gamma_{133}^2}{K_{33}}, \quad \gamma_{31} = \mathcal{A}_{3131} - \frac{\Gamma_{133}^2}{K_{33}}, \quad \gamma_{32} = \mathcal{A}_{3232},$$

$$\xi_1 = -\left(\frac{\Gamma_{122}}{K_{22}}\frac{n^2}{\gamma_{12}} + \frac{\Gamma_{133}}{K_{33}}\frac{k^2r^2}{\gamma_{13}}\right)\tau_{rr},$$

$$\xi_2 = -\left(\frac{n^2}{K_{22}} + \frac{\Gamma_{122}^2}{K_{22}^2}\frac{n^2}{\gamma_{12}} + \frac{k^2r^2}{K_{33}} + \frac{\Gamma_{133}^2}{K_{33}^2}\frac{k^2r^2}{\gamma_{13}}\right),$$

$$\beta_{12} = \frac{1}{2}\left(\mathcal{A}_{1111} + \mathcal{A}_{2222} - 2\mathcal{A}_{1122} - 2\mathcal{A}_{1221} + \frac{2\Gamma_{122}^2}{K_{22}}\right),$$

$$\beta_{13} = \frac{1}{2}\left(\mathcal{A}_{1111} + \mathcal{A}_{3333} - 2\mathcal{A}_{1133} - 2\mathcal{A}_{1331} + \frac{2\Gamma_{133}^2}{K_{33}}\right),$$

$$\kappa_{11} = 2(\gamma_{12} - \tau_{rr} + \beta_{12}) + n^2\left[\gamma_{21} - \frac{(\gamma_{12}-\tau_{rr})^2}{\gamma_{12}}\right] + k^2r^2\left[\gamma_{31} - \frac{(\gamma_{13}-\tau_{rr})^2}{\gamma_{13}}\right],$$

$$\kappa_{12} = n\left(\gamma_{12} + \gamma_{21} + 2\beta_{12} - \frac{\tau_{rr}^2}{\gamma_{12}}\right),$$

$$\kappa_{13} = kr\left(\mathcal{A}_{1111} + \mathcal{A}_{2233} - \mathcal{A}_{1122} - \mathcal{A}_{1133} + p\right),$$

$$\kappa_{22} = 2n^2(\gamma_{12} - \tau_{rr} + \beta_{12}) + \gamma_{21} - \frac{(\gamma_{12}-\tau_{rr})^2}{\gamma_{12}} + k^2r^2\gamma_{32},$$

$$\kappa_{23} = nkr\left(\mathcal{A}_{1111} + \mathcal{A}_{2233} + \mathcal{A}_{2332} - \mathcal{A}_{1122} - \mathcal{A}_{1133} + 2p\right),$$

$$\kappa_{33} = 2k^2r^2\left(\gamma_{13} - \tau_{rr} + \beta_{13}\right) + n^2\gamma_{23}. \tag{A.3}$$

Here p is a Lagrange multiplier associated with the incompressibility constraint of the material, $\mathcal{A}_{ijkl}, \Gamma_{ijk}$ and K_{ij} $(i,j,k,l = 1,2,3)$ are components of the fourth-, third- and second-order effective electroelastic moduli tensors $\boldsymbol{\mathcal{A}}$, $\boldsymbol{\Gamma}$ and $\boldsymbol{K}$, which are listed in Appendix B for reference.

Appendix B. Non-zero electroelastic moduli

For the considered problem, the non-zero components of the instantaneous electroelastic moduli read [32,43]

$$\begin{aligned}\mathcal{A}_{01111} =& 2\lambda^{-4}\lambda_z^{-4}\left\{\lambda^4\left[2\Omega_{22} + \lambda_z^2\left(\Omega_2 + 4\Omega_{25}D_r^2\right) + \lambda_z^4 D_r^2\left(\Omega_5 + 2\Omega_{55}D_r^2\right)\right]\right.\\ &+2\left[\Omega_{11} + \lambda_z^4\Omega_{22} + 2\lambda_z^2\left(\Omega_{12} + 2\Omega_{26}D_r^2\right) + 4D_r^2\left(\Omega_{16} + \Omega_{66}D_r^2\right)\right]\\ &\left.+\lambda^2\lambda_z^4\left(\Omega_2 + 4\Omega_{25}D_r^2\right) + 4\lambda^2\left(\Omega_{12} + 2\Omega_{26}D_r^2\right)\right.\end{aligned}$$

$$
\begin{aligned}
&+\lambda^2\lambda_z^2\left[\Omega_1+4\Omega_{22}+8\Omega_{56}D_r^4+D_r^2\left(4\Omega_{15}+6\Omega_6\right)\right]\},\\
\mathcal{A}_{01122}=&4\lambda^{-2}\lambda_z^{-4}\left\{\Omega_{12}+\lambda_z^2\Omega_{22}+\lambda^4\lambda_z^2\left[\Omega_{12}+\lambda_z^2\Omega_{22}\right.\right.\\
&+\lambda_z^2D_r^2\left(\Omega_{15}+\lambda_z^2\Omega_{25}\right)\left.\left.\right]+2\Omega_{26}D_r^2\right.\\
&+\lambda^2\left[\Omega_{22}+\lambda_z^6\Omega_{22}+\lambda_z^2\Omega_{11}+\lambda_z^2\Omega_2+\lambda_z^2D_r^2\left(2\Omega_{16}+\Omega_{25}\right)\right.\\
&\left.\left.+2\lambda_z^4\left(\Omega_{12}+\Omega_{26}D_r^2\right)\right]\right\},\\
\mathcal{A}_{01133}=&4\lambda^{-4}\lambda_z^{-2}\left\{\Omega_{12}+\lambda^2\Omega_{22}+\lambda^2\lambda_z^4\left[\Omega_{12}+\lambda^2\Omega_{22}\right.\right.\\
&+\lambda^2D_r^2\left(\Omega_{15}+\lambda^2\Omega_{25}\right)\left.\left.\right]+2\Omega_{26}D_r^2\right.\\
&+\lambda_z^2\left[\Omega_{22}+\lambda^6\Omega_{22}+\lambda^2\Omega_{11}+\lambda^2\Omega_2+\lambda^2D_r^2\left(2\Omega_{16}+\Omega_{25}\right)\right.\\
&\left.\left.+2\lambda^4\left(\Omega_{12}+\Omega_{26}D_r^2\right)\right]\right\},\\
\mathcal{A}_{01212}=&2\lambda^{-2}\lambda_z^{-2}\left\{\Omega_1+2\Omega_6D_r^2+\lambda_z^2\left[\Omega_2+\lambda^2D_r^2\left(\Omega_5+\lambda^2\Omega_6\right)\right]\right\},\\
\mathcal{A}_{01313}=&2\lambda^{-2}\lambda_z^{-2}\left\{\Omega_1+2\Omega_6D_r^2+\lambda^2\left[\Omega_2+\lambda_z^2D_r^2\left(\Omega_5+\lambda_z^2\Omega_6\right)\right]\right\},\\
\mathcal{A}_{01221}=&-2\lambda_z^{-2}\Omega_2+2\lambda^2\Omega_6D_r^2,\quad \mathcal{A}_{01331}=-2\lambda^{-2}\Omega_2+2\lambda_z^2\Omega_6D_r^2,\\
\mathcal{A}_{02121}=&2\lambda^2\left(\Omega_1+\lambda_z^2\Omega_2+\Omega_6D_r^2\right),\quad \mathcal{A}_{03131}=2\lambda_z^2\left(\Omega_1+\lambda^2\Omega_2+\Omega_6D_r^2\right),\\
\mathcal{A}_{02222}=&2\lambda_z^{-4}\left[\lambda_z^2\Omega_2+2\Omega_{22}+\lambda^2\left(\lambda_z^4\Omega_1+4\lambda_z^4\Omega_{12}+\lambda_z^6\Omega_2+4\lambda_z^4\Omega_{22}\right)\right.\\
&\left.+2\lambda^4\lambda_z^4\left(\Omega_{11}+2\lambda_z^2\Omega_{12}+\lambda_z^4\Omega_{22}\right)\right],\\
\mathcal{A}_{02233}=&4\lambda^{-2}\lambda_z^{-2}\left[\Omega_{22}+\lambda^4\lambda_z^2\left(\lambda_z^4\Omega_{12}+\lambda_z^2\Omega_{11}+\lambda_z^2\Omega_2+\Omega_{22}\right)\right.\\
&\left.+\lambda^6\lambda_z^4\left(\Omega_{12}+\lambda_z^2\Omega_{22}\right)+\lambda^2\left(2\lambda_z^2\Omega_{12}+\lambda_z^4\Omega_{22}\right)\right],\\
\mathcal{A}_{02323}=&2\lambda^2\Omega_1+2\lambda_z^{-2}\Omega_2,\quad \mathcal{A}_{02332}=-2\lambda^2\lambda_z^2\Omega_2,\\
\mathcal{A}_{03232}=&2\lambda_z^2\Omega_1+\lambda^{-2}\Omega_2,\\
\mathcal{A}_{03333}=&2\lambda^{-4}\left[\lambda^2\Omega_2+2\Omega_{22}+\lambda_z^2\left(\lambda^4\Omega_1+4\lambda^4\Omega_{12}+\lambda^6\Omega_2+4\lambda^4\Omega_{22}\right)\right.\\
&\left.+2\lambda^4\lambda_z^4\left(\Omega_{11}+2\lambda^2\Omega_{12}+\lambda^4\Omega_{22}\right)\right],
\end{aligned}
\tag{B.1}
$$

$$
\begin{aligned}
\Gamma_{0111}=&4\lambda^{-4}\lambda_z^{-4}D_r\left\{\Omega_{16}+\lambda_z^2\Omega_{26}+\lambda^6\lambda_z^4\left(\Omega_{24}+\lambda_z^2\Omega_{45}D_r^2\right)\right.\\
&+\lambda^4\lambda_z^z\left[\lambda_z^4\Omega_{24}+\Omega_{25}+\lambda_z^2\left(\Omega_{14}+\Omega_5+2\Omega_{46}D_r^2+\Omega_{55}D_r^2\right)\right]\\
&\left.+2\Omega_{66}D_r^2+\lambda^2\left[\lambda_z^4\Omega_{25}+\Omega_{26}+\lambda_z^2\left(\Omega_{15}+3\Omega_{56}D_r^2+2\Omega_6\right)\right]\right\},\\
\Gamma_{0122}=&2\lambda^{-2}\lambda_z^{-2}D_r\left[\lambda^2\lambda_z^2\Omega_5+\left(1+\lambda^4\lambda_z^2\right)\Omega_6\right],\\
\Gamma_{0133}=&2\lambda^{-2}\lambda_z^{-2}D_r\left[\lambda^2\lambda_z^2\Omega_5+\left(1+\lambda^2\lambda_z^4\right)\Omega_6\right],\\
\Gamma_{0221}=&4\lambda^{-2}\lambda_z^{-4}D_r\left[\lambda^6\lambda_z^6\left(\Omega_{14}+\lambda_z^2\Omega_{24}\right)+\lambda^4\lambda_z^4\left(\Omega_{15}+\Omega_{24}+\lambda_z^2\Omega_{25}\right)\right.\\
&\left.+\Omega_{26}+\lambda^2\lambda_z^2\left(\Omega_{16}+\Omega_{25}+\lambda_z^2\Omega_{26}\right)\right],\\
\Gamma_{0331}=&4\lambda^{-4}\lambda_z^{-2}D_r\left[\lambda^6\lambda_z^6\left(\Omega_{14}+\lambda^2\Omega_{24}\right)+\lambda^4\lambda_z^4\left(\Omega_{15}+\Omega_{24}+\lambda^2\Omega_{25}\right)\right.\\
&\left.+\Omega_{26}+\lambda^2\lambda_z^2\left(\Omega_{16}+\Omega_{25}+\lambda^2\Omega_{26}\right)\right],
\end{aligned}
\tag{B.2}
$$

$$
\begin{aligned}
K_{011}=&\lambda^{-4}\lambda_z^{-4}\left[2\lambda^2\lambda_z^2\left(\lambda^2\lambda_z^2\Omega_5+\Omega_6+\lambda^4\lambda_z^4\Omega_4\right)\right.\\
&+4D_r^2\left(\lambda^8\lambda_z^8\Omega_{44}+2\lambda^6\lambda_z^6\Omega_{45}+2\lambda^4\lambda_z^4\Omega_{46}\right.\\
&\left.\left.+\lambda^4\lambda_z^4\Omega_{55}+2\lambda^2\lambda_z^2\Omega_{56}+\Omega_{66}\right)\right],\\
K_{022}=&2\left(\Omega_5+\lambda^2\Omega_6+\lambda^{-2}\Omega_4\right),\quad K_{033}=2\left(\Omega_5+\lambda_z^2\Omega_6+\lambda_z^{-2}\Omega_4\right),
\end{aligned}
\tag{B.3}
$$

where $\Omega_{ij}=\partial^2\Omega/\partial I_i\partial I_j$, and Ω is the energy function of the material in terms of the following five scalar invariants

$$
I_1=\mathrm{tr}\boldsymbol{c},\quad I_2=\mathrm{tr}\left(\boldsymbol{c}^{-1}\right),\quad I_4=\boldsymbol{D}_l\cdot\boldsymbol{D}_l,\quad I_5=\boldsymbol{D}_l\cdot\boldsymbol{c}\boldsymbol{D}_l,\quad I_6=\boldsymbol{D}_l\cdot\boldsymbol{c}^2\boldsymbol{D}_l,
\tag{B.4}
$$

where $\boldsymbol{c}=\boldsymbol{F}^{\mathrm{T}}\boldsymbol{F}$ is the right Cauchy–Green deformation tensor and $\boldsymbol{D}_l=\boldsymbol{F}^{-1}\boldsymbol{D}$ is the nominal electric displacement.

References

[1] S. Kim, C. Laschi, B. Trimmer, Soft robotics: a bioinspired evolution in robotics, Trends Biotechnol. 31 (5) (2013) 287–294.

[2] A.A. Stokes, R.F. Shepherd, S.A. Morin, F. Ilievski, G.M. Whitesides, A hybrid combining hard and soft robots, Soft Robot. 1 (1) (2014) 70–74.

[3] K. Kumar, J. Liu, C. Christianson, M. Ali, M.T. Tolley, J. Aizenberg, D.E. Ingber, J.C. Weaver, K. Bertoldi, A biologically inspired, functionally graded end effector for soft robotics applications, Soft Robot. 4 (4) (2017) 317–323.

[4] N.W. Bartlett, M.T. Tolley, J.T. Overvelde, J.C. Weaver, B. Mosadegh, K. Bertoldi, G.M. Whitesides, R.J. Wood, A. 3D-printed, Functionally graded soft robot powered by combustion, Science 349 (6244) (2015) 161–165.

[5] A. Dorfmann, R.W. Ogden, Nonlinear Theory of Electroelastic and Magnetoelastic Interactions, Springer, New York, 2014.

[6] R.M. McMeeking, C.M. Landis, Electrostatic forces and stored energy for deformable dielectric materials, J. Appl. Mech. 72 (4) (2005) 581–590.

[7] Z. Suo, X. Zhao, W.H. Greene, A nonlinear field theory of deformable dielectrics, J. Mech. Phys. Solids 56 (2) (2008) 467–486.

[8] F. Carpi, D. De Rossi, R. Kornbluh, R.E. Pelrine, P. Sommers-Larsen, Dielectric Elastomers as Electromechanical Transducers: Fundamentals, Materials, Devices, Models and Applications of an Emerging Electroactive Polymer Technology, Elsevier, Science, 2011.

[9] S. Rosset, H.R. Shea, Small, fast, and tough: Shrinking down integrated elastomer transducers, Appl. Phys. Rev. 3 (3) (2016) 031105.

[10] I.A. Anderson, T.A. Gisby, T.G. McKay, B.M. O'Brien, E.P. Calius, Multi-functional dielectric elastomer artificial muscles for soft and smart machines, J. Appl. Phys. 112 (4) (2012) 041101.

[11] D.L. Henann, S.A. Chester, K. Bertoldi, Modeling of dielectric elastomers: design of actuators and energy harvesting devices, J. Mech. Phys. Solids 61 (10) (2013) 2047–2066.

[12] X. Zhao, Q. Wang, Harnessing large deformation and instabilities of soft dielectrics: theory, experiment, and application, Appl. Phys. Rev. 1 (2) (2014) 021304.

[13] B. Wu, W. Zhou, R. Bao, W. Chen, Tuning elastic waves in soft phononic crystal cylinders via large deformation and electromechanical coupling, J. Appl. Mech. 85 (3) (2018) 031004.

[14] W. Zhou, Y. Su, W. Chen, C.W. Lim, Voltage-controlled quantum valley hall effect in dielectric membrane-type acoustic metamaterials, Int. J. Mech. Sci. 172 (2020) 105368.

[15] G. Bossis, C. Abbo, S. Cutillas, S. Lacis, C. Métayer, Electroactive and electro structured elastomers, Internat. J. Modern Phys. B 15 (6–7) (2001) 564–573.

[16] J. Zhu, H. Stoyanov, G. Kofod, Z. Suo, Large deformation and electromechanical instability of a dielectric elastomer tube actuator, J. Appl. Phys. 108 (7) (2010) 074113.

[17] R. Pelrine, R. Kornbluh, Q. Pei, J. Joseph, High-speed electrically actuated elastomers with strain greater than 100%, Science 287 (5454) (2000) 836–839.

[18] R.M. Mahamood, E.T. Akinlabi, M. Shukla, S. Pityana, Functionally graded material: an overview, in: Proceedings of the World Congress on Engineering 2012, Vol. III, WCE 2012, London, UK, 2012.

[19] E. Bilgili, B. Bernstein, H. Arastoopour, Influence of material non homogeneity on the shearing response of a neo hookean slab, Rubber Chem. technol. 75 (2) (2002) 347–363.

[20] X. Wang, M. Jiang, Z. Zhou, J. Gou, D. Hui, 3D Printing of polymer matrix composites: A review and prospective, Composites B 110 (2017) 442–458.

[21] Y. Chen, B. Wu, Y. Su, W. Chen, Effects of strain stiffening and electrostriction on tunable elastic waves in compressible dielectric elastomer laminates, Int. J. Mech. Sci. (2020) 105572.

[22] W. Pang, X. Cheng, H. Zhao, X. Guo, Z. Ji, G. Li, Y. Liang, Z. Xue, H. Song, F. Zhang, Z. Xu, Electro-mechanically controlled assembly of reconfigurable 3D mesostructures and electronic devices based on dielectric elastomer platforms, Natl. Sci. Rev. 7 (2) (2020) 342–354.

[23] R.A. Toupin, The elastic dielectric, J. Ration. Mech. Anal. 5 (6) (1956) 849–915.

[24] L.D. Landau, E.M. Lifshitz, Electrodynamics of Electromagnetic Solids, Pergamon, Oxford, 1960.

[25] H.F. Tiersten, On the nonlinear equations of thermo-electroelasticity, Internat. J. Engrg. Sci. 9 (7) (1971) 587–604.

[26] G.A. Maugin, Continuum Mechanics of Electromagnetic Solids, Elsevier, 1988.

[27] E. Baesu, D. Fortune, E. Soós, Incremental behaviour of hyperelastic dielectrics and piezoelectric crystals, Z. Angew. Math. Phys. 54 (1) (2003) 160–178.

[28] A. Dorfmann, R.W. Ogden, Electroelastic waves in a finitely deformed electroactive material, IMA J. Appl. Math. 75 (4) (2010) 603–636.

[29] G. Shmuel, G. deBotton, Axisymmetric wave propagation in finitely deformed dielectric elastomer tubes, Proc. R. Soc. A 469 (2155) (2013) 20130071.

[30] P.I. Galich, S. Rudykh, Shear wave propagation and band gaps in finitely deformed dielectric elastomer laminates: long wave estimates and exact solution, J. Appl. Mech. 84 (9) (2017) 091002.

[31] Y. Wang, Z. Li, W. Chen, C. Zhang, J. Zhu, Free vibration and active control of pre-stretched multilayered electroactive plates, Int. J. Solids Struct. 180 (2019) 108–124.

[32] Y. Su, B. Wu, W. Chen, M. Destrade, Finite bending and pattern evolution of the associated instability for a dielectric elastomer slab, Int. J. Solids Struct. 158 (2019) 191–209.

[33] Y. Su, W. Chen, M. Destrade, Tuning the pull-in instability of soft dielectric elastomers through loading protocols, Internat. J. Non-Linear Mech. 113 (2019) 62–66.

[34] M. Yamanouchi, M. Koizumi, T. Hirai, I. Shiota, Proc. First Int. Symp. on Functionally Gradient Materials, FGM Forum, Tokyo, Japan, 1990.

[35] N.J. Pagano, Stress fields in composite laminates, Int. J. Solids Struct. 14 (5) (1978) 385–400.

[36] J. Yang, H. Shen, Dynamic response of initially stressed functionally graded rectangular thin plates, Compos. Struct. 54 (4) (2001) 497–508.

[37] J. Yang, K.M. Liew, S. Kitipornchai, Imperfection sensitivity of the post-buckling behavior of higher-order shear deformable functionally graded plates, Int. J. Solids Struct. 43 (17) (2006) 5247–5266.
[38] V. Birman, L.W. Byrd, Modeling and analysis of functionally graded materials and structures, Appl. Mech. Rev. 60 (1–6) (2007) 195–216.
[39] L. Ke, J. Yang S. Kitipornchai, Y. Wang, Electro-mechanical frictionless contact behavior of a functionally graded piezoelectric layered half-plane under a rigid punch, Int. J. Solids Struct. 45 (11–12) (2008) 3313–3333.
[40] W. Chen, D. Liu, S. Kitipornchai, J. Yang, Bifurcation of pressurized functionally graded elastomeric hollow cylinders, Composites B 109 (2017) 259–276.
[41] B. Wu, Y. Su, D. Liu, W. Chen, C. Zhang, On propagation of axisymmetric waves in pressurized functionally graded elastomeric hollow cylinders, J. Sound Vib. 421 (2018) 17–47.
[42] R.W. Ogden, Non-Linear Elastic Deformations, Dover, New York, 1997.
[43] B. Wu, Y. Su, W. Chen, C. Zhang, On guided circumferential waves in soft electroactive tubes under radially inhomogeneous biasing fields, J. Mech. Phys. Solids 99 (2017) 116–145.
[44] L. Dorfmann, R.W. Ogden, Instabilities of an electroelastic plate, Internat. J. Engrg. Sci. 77 (2014) 79–101.
[45] A. Dorfmann, R.W. Ogden, Nonlinear electroelastic deformations, J. Elasticity 82 (2) (2006) 99–127.
[46] J. Huang, T. Li, C.C. Foo, J. Zhu, D.R. Clarke, Z. Suo, Giant, voltage-actuated deformation of a dielectric elastomer under dead load, Appl. Phys. Lett. 100 (2012) 041911.
[47] Y. Su, H.C. Broderick, W. Chen, M. Destrade, Wrinkles in soft dielectric plates, J. Mech. Phys. Solids 119 (2018) 298–318.
[48] L. He, J. Lou, J. Du, J. Wang, Finite bending of a dielectric elastomer actuator and pre-stretch effects, Int. J. Mech. Sci. 122 (2017) 120–128.
[49] A. Melnikov, L. Dorfmann, R.W. Ogden, Bifurcation of finitely deformed thick-walled electroelastic spherical shells subject to a radial electric field, Internat. J. Non-Linear Mech. 121 (2020) 103429.
[50] Y. Su, W. Zhou, W. Chen, C. Lü, On buckling of a soft incompressible electroactive hollow cylinder, Int. J. Solids Struct. 97 (2016) 400–416.
[51] M. Destrade, A. Ní Annaidh, C.D. Coman, Bending instabilities of soft biological tissues, Int. J. Solids Struct. 46 (25–26) (2009) 4322–4330.
[52] X. Zhao, Z. Suo, Method to analyze electromechanical stability of dielectric elastomers, Appl. Phys. Lett. 91 (6) (2007) 061921.
[53] K.H. Stark, C.G. Garton, Electric strength of irradiated polythene, Nature 176 (4495) (1955) 1225–1226.
[54] Y. Su, B. Wu, W. Chen, C. Lü, Optimizing parameters to achieve giant deformation of an incompressible dielectric elastomeric plate, Extreme Mech. Lett. 22 (2018) 60–68.
[55] A. Dorfmann, D.M. Haughton, Stability and bifurcation of compressed elastic cylindrical tubes, Internat. J. Engrg. Sci. 44 (18–19) (2006) 1353–1365.
[56] M.A. Biot, Exact theory of buckling of a thick slab, Appl. Sci. Res. A 12 (2) (1963) 183–198.
[57] Y. Du, C. Lü, C. Liu, Z. Han, J. Li, W. Chen, S. Qu, M. Destrade, Prescribing patterns in growing tubular soft matter by initial residual stress, Soft Matter 15 (42) (2019) 8468–8474.
[58] L. Wang, Axisymmetric instability of soft elastic tubes under axial load and surface tension, Int. J. Solids Struct. 191 (2020) 341–350.